The excitation of spiral density waves through turbulent fluctuations in accretion discs I: WKBJ theory

T. Heinemann[1] and J. C. B. Papaloizou[1]

[1] *University of Cambridge, Wilberforce Road, Cambridge CB3 0WA*

30 April 2009

ABSTRACT

We study and elucidate the mechanism of spiral density wave excitation in a differentially rotating flow with turbulence which could result from the magneto-rotational instability. We formulate a set of wave equations with sources that are only non-zero in the presence of turbulent fluctuations. We solve these in a shearing box domain, subject to the boundary conditions of periodicity in shearing coordinates, using a WKBJ method. It is found that, for a particular azimuthal wave length, the wave excitation occurs through a sequence of regularly spaced swings during which the wave changes from leading to trailing form. This is a generic process that is expected to occur in shearing discs with turbulence. Trailing waves of equal amplitude propagating in opposite directions are produced, both of which produce an outward angular momentum flux that we give expressions for as functions of the disc parameters and azimuthal wave length.

By solving the wave amplitude equations numerically we justify the WKBJ approach for a Keplerian rotation law for all parameter regimes of interest. In order to quantify the wave excitation completely the important wave source terms need to be specified. Assuming conditions of weak nonlinearity, these can be identified and are associated with a quantity related to the potential vorticity, being the only survivors in the linear regime. Under the additional assumption that the source has a flat power spectrum at long azimuthal wave lengths, the optimal azimuthal wave length produced is found to be determined solely by the WKBJ response and is estimated to be $2\pi H$, with H being the nominal disc scale height. In a following paper by Heinemann & Papaloizou, we perform direct three dimensional simulations and compare results manifesting the wave excitation process and its source with the assumptions made and the theory developed here in detail, finding excellent agreement.

Key words: accretion, accretion discs – turbulence – waves

1 INTRODUCTION

Accretion discs are ubiquitous in astrophysics, occurring in close binary systems, active galactic nuclei and around protostars (see e.g. Papaloizou & Lin 1995; Lin & Papaloizou 1996, for reviews). Ever since their importance was first realized it has been clear that some form of turbulence is necessary to provide the anomalous angular momentum transport implied by observed luminosities and inferred accretion rates. This has usually been parametrised using the Shakura & Syunyaev (1973) α-parametrisation.

The most likely source of turbulence is through the magneto-rotational instability (MRI) (see Balbus & Hawley 1991, 1998). Both local and global simulations that display sustained MRI turbulence have been performed with and without net flux. In all cases prolific spiral density (SD) wave excitation has been noted (e.g. Gardiner & Stone 2005

in the local case and Armitage 1998 in the global case). These waves may be crucial for explaining various phenomena in accretion disk systems. In the context of protoplanetary disks for instance, it has recently been suggested that stochastic gravitational forces derived from density variations due to SD waves may play an important role in driving the migration of low mass protoplanets (Nelson & Papaloizou 2004; Nelson 2005). This possibly remains a viable mechanism even in so-called dead zones where the ionization fraction is too low for MHD turbulence to occur, see the recent simulations by Oishi, Mac Low & Menou 2007. In general, SD waves may lead to significantly enhanced angular momentum transport in magnetically inactive regions of accretion disks. It is therefore important to gain an understanding of the processes leading to the excitation of spiral density waves, how generic the phenomenon is, and how the wave amplitudes scale with physical parameters.

In order to do this, we assume weakly nonlinear conditions, under which the important source terms for exciting the SD waves are expected to be proportional to what we call the pseudo potential vorticity (PPV), which is equal to the potential vorticity to linear order but differs from it in the nonlinear regime. The potentially important role that PPV plays for the excitation of SD waves in rotating shear flows has been recognised in earlier work (see e.g. Chagelishvili et al. 1997). These authors found by numerically integrating the linearised equations of motion of compressible, plane Couette flow that there exists a linear mode coupling between specified vortical perturbations and (free) SD waves that leads to efficient excitation of the latter (see also Bodo et al. 2005 for a similar study in the context of accretion disks). However, the possibility of the generation of vortical perturbations through the action of turbulence has not yet been fully assessed.

It is the purpose of this paper to develop a mathematically rigorous theory of the excitation of SD waves within the WKBJ framework. Our approach is inspired by the work of Vanneste & Yavneh (2004) who developed an analogous theory for small amplitude inertia-gravity waves in a local, quasi-geostrophic model of the Earth's atmosphere. Apart from illuminating the excitation process of SD waves in rotating shear flows by putting it on a firm mathematical basis, the theory also enables us to calculate the amplitude of the excited waves and the associated angular momentum transport explicitly.

In a following paper (Heinemann & Papaloizou 2009, paper II) we perform numerical simulations which to study SD wave excitation in MRI driven turbulence (see also Gardiner & Stone 2005; Shen et al. 2006) and make detailed comparisons to the WKBJ theory presented here. In this scenario, magnetically dominated turbulent stresses cause vortical perturbations which then in turn lead to the excitation of the observed SD waves. The role that turbulent stresses play is thus indirect. In this aspect the excitation process differs from that considered in Lighthill's theory of aerodynamic noise generation (Lighthill 1952).

The plan of this paper is as follows: In section 2 we describe the shearing box model, giving the basic equations and defining the background shear flow in which the hydromagnetic turbulence responsible for the SD wave excitation, is generated. In section 3 we derive equations describing the excitation of SD waves. These take the form of linear wave equations with both linear and nonlinear source terms that are determined by the turbulence. We focus on waves that are nearly independent of the vertical coordinate which have been found to dominate in simulations carried out in paper II and which can be dealt with using a vertical averaging procedure. We formulate the law of conservation of angular momentum for linear, non-dissipative SD waves and derive a convenient expression for the average radial flux which we later use to estimate the angular momentum flux arising due to the excited waves.

In section 4 we go on to develop the WKBJ theory of wave excitation. A Fourier analysis is carried out enabling each azimuthal wave number k_y to be considered separately. The WKBJ theory applies to a shearing box for which the boundary conditions are the imposition of periodicity in shearing coordinates and involves a sequence of excitations uniformly spaced and localized in time, during which the

wave swings from leading to trailing. The wave amplitude and wave action produced in a swing are calculated from a WKBJ formalism involving the evaluation of integrals along anti-Stokes lines.

We compare the results derived from asymptotic theory to results obtained by numerically integrating the ordinary differential equations describing the evolution of the appropriate Fourier amplitude. We find excellent agreement between these approaches. This agreement persists under all conditions of interest. This is in spite of the fact that asymptotic theory formally requires a parameter depending on the azimuthal wave number to be small. Finally we discuss our results in Section 5.

2   THE SHEARING BOX MODEL

2.1   Basic set up and equations

We consider a conducting gas in the shearing box approximation (Goldreich & Lynden-Bell 1965). A Cartesian coordinate system (x, y, z) with origin at the centre of the box is adopted. The system rotates with angular velocity $\boldsymbol{\Omega} = \Omega \boldsymbol{e}_z$, with $\boldsymbol{e}_z$ being the unit vector in the z-direction. This coincides with the angular velocity of the centre of the box, taken to be in a circular orbit. In the Keplerian case this is about a central point mass. The lengths of the sides of the box in the three coordinate directions are (L_x, L_y, L_z) and vertical stratification is neglected.

The basic equations are those of MHD for an isothermal gas, i.e. the continuity equation

$$\frac{\partial \rho}{\partial t} + \nabla \cdot (\rho \boldsymbol{v}) = 0,$$

the momentum equation

$$\frac{\partial (\rho \boldsymbol{v})}{\partial t} = -c^2 \nabla \rho - 2\boldsymbol{\Omega} \times \rho \boldsymbol{v} - \rho \nabla \Phi + \nabla \cdot \boldsymbol{T}' + \nabla \cdot (2\rho \nu \boldsymbol{S})$$

and the induction equation

$$\frac{\partial \boldsymbol{B}}{\partial t} = \nabla \times (\boldsymbol{v} \times \boldsymbol{B} - \eta \nabla \times \boldsymbol{B})$$

where ρ is the density, the velocity is $\boldsymbol{v} = (v_x, v_y, v_z)$, the isothermal sound speed is c, the magnetic field is $\boldsymbol{B} = (B_x, B_y, B_z)$, the nonlinear stress tensor $\boldsymbol{T}'$ has components

$$T'_{ij} = B_i B_j - \delta_{ij} \boldsymbol{B}^2/2 - \rho v_i v_j,$$

and $\boldsymbol{S}$ is the traceless rate-of-strain tensor whose components are given by

$$S_{ij} = \frac{1}{2} \left(\frac{\partial v_i}{\partial x_j} + \frac{\partial v_j}{\partial x_i} - \frac{2}{3} \delta_{ij} \nabla \cdot \boldsymbol{v} \right).$$

The kinematic viscosity is ν, the resistivity is η, and the combined gravitational and centrifugal potential is given by

$$\Phi = -q\Omega^2 x^2,$$

where for a Keplerian flow the constant $q = 3/2$.

The isothermal MHD equations admit the definition of a characteristic length scale $H = c/\Omega$, which we will refer to as the nominal disc scale height even though we have neglected vertical stratification.

2.2 Equations for deviations from the steady state and boundary conditions

The background state is taken to have uniform density ρ_0, zero magnetic field and a linear shear corresponding to the velocity

$$\boldsymbol{v}_0 = -q\Omega x \boldsymbol{e}_y.$$

As we are interested in wave propagation we work in terms of velocity deviations from the background shear, $\boldsymbol{u} = \boldsymbol{v} - \boldsymbol{v}_0$, which we use to define the linear momentum density per unit volume $\boldsymbol{p} = \rho\boldsymbol{u}$. In terms of ρ and $\boldsymbol{p}$ the governing equations now read

$$\mathcal{D}\rho + \nabla \cdot \boldsymbol{p} = 0, \tag{1}$$

$$\mathcal{D}\boldsymbol{p} = -c^2\nabla\rho - 2\boldsymbol{\Omega}\times\boldsymbol{p} + q\Omega p_x\boldsymbol{e}_y + \nabla\cdot\boldsymbol{T} + \nabla\cdot(2\rho\nu\boldsymbol{S}), \tag{2}$$

$$\mathcal{D}\boldsymbol{B} = \nabla\times(\boldsymbol{u}\times\boldsymbol{B} - \eta\nabla\times\boldsymbol{B}) - q\Omega B_x\boldsymbol{e}_y \tag{3}$$

where the differential operator

$$\mathcal{D} = \frac{\partial}{\partial t} - q\Omega x\frac{\partial}{\partial y} \tag{4}$$

accounts for advection by the linear shear. Note that here, the nonlinear stress tensor

$$T_{ij} = B_iB_j - \delta_{ij}\boldsymbol{B}^2/2 - \rho u_i u_j \tag{5}$$

only contains products of deviations from the background state.

We consider equations (1) to (3) to be subject to periodic boundary conditions in 'Lagrangian' (or 'shearing') coordinates given by

$$x' = x, \ y' = y + q\Omega tx, \ z' = z, \ \text{and} \ t' = t, \tag{6}$$

transformation to which removes the explicit x-dependence contained in (4) – albeit at the expense of an explicit time dependence[1]. Re-expressed in 'Eulerian' coordinates (x, y, z, t) the radial boundary condition for any fluid variable f then reads

$$f(x + L_x, y - q\Omega tL_x, z, t) = f(x, y, z, t)$$

while the azimuthal and vertical boundary conditions are simply

$$f(x, y + L_y, z, t) = f(x, y, z, t)$$

and

$$f(x, y, z + L_z, t) = f(x, y, z, t),$$

respectively.

3 WAVE EQUATIONS WITH SOURCES

In order to proceed we develop equations for the deviation of the state variables from their background state in order to obtain wave equations with sources. These can then be used to study the excitation of SD waves explicitly. It is known that SD waves can propagate in a strictly isothermal box with no dependence on the vertical coordinate (see Fromang

[1] Without loss of generality we have assumed that the two coordinate systems coincide at $t = 0$.

& Papaloizou 2007) and we have found that such waves are the ones predominantly excited in our simulations presented in paper II. We therefore vertically average equations (1) and (2), which then become equations for the vertical averages of the state variables such as $\boldsymbol{p}$ and ρ, in order to describe such waves. When periodic boundary conditions in z are adopted this can be done without approximation and it is equivalent to adopting $k_z = 0$ when Fourier transforms are considered. Proceeding in this way, we denote the vertical average of a quantity f by use of angle brackets as $\langle f\rangle_z$.

To further simplify the analysis we consider the inviscid limit of the shearing box equations, which then become

$$\mathcal{D}\langle\rho\rangle_z + \partial_x\langle p_x\rangle_z + \partial_y\langle p_y\rangle_z = 0 \tag{7a}$$

$$\mathcal{D}\langle p_x\rangle_z + c^2\partial_x\langle\rho\rangle_z - 2\Omega\langle p_y\rangle_z = \langle\mathfrak{N}_x\rangle_z \tag{7b}$$

$$\mathcal{D}\langle p_y\rangle_z + c^2\partial_y\langle\rho\rangle_z + (2-q)\Omega\langle p_x\rangle_z = \langle\mathfrak{N}_y\rangle_z \tag{7c}$$

where we introduced the short-hand $\mathfrak{N} = \nabla\cdot\boldsymbol{T}$. At this point we note that in the zero net flux case considered here, the magnetic field enters the momentum equation only through the nonlinear stress tensor (5) so that it will not affect the description of linear SD waves.

Acting on (7c) with $\mathcal{D}$ and rearranging terms yields

$$(\mathcal{D}^2 - c^2\nabla^2 + \kappa^2)\langle p_y\rangle_z =$$
$$-c^2\partial_x\langle\zeta\rangle_z + (q-2)\Omega\langle\mathfrak{N}_x\rangle_z + \mathcal{D}\langle\mathfrak{N}_y\rangle_z \tag{8}$$

where $\kappa^2 = 2(2-q)\Omega^2$ is the square of the epicyclic frequency and

$$\zeta = \partial_x p_y - \partial_y p_x + (q-2)\Omega\rho,$$

which we shall call the pseudo potential vorticity (PPV). To linear order, the variation of PPV is equal to the variation of potential vorticity (PV),

$$Q = \frac{\partial_x u_y - \partial_y u_x + (2-q)\Omega}{\rho},$$

(see Johnson & Gammie 2005). Written out explicitly, we have

$$\zeta - \zeta_0 = \rho_0^2(Q - Q_0) + \text{nonlinear terms},$$

where

$$\zeta_0 = (q-2)\Omega\rho_0 \quad \text{and} \quad Q_0 = \frac{(2-q)\Omega}{\rho_0}$$

are the steady state background values of PPV and PV, respectively. For disturbances with $k_z = 0$ and given a barotropic equation of state, PV is an exactly conserved quantity whereas PPV varies due to nonlinear stresses,

$$\mathcal{D}\langle\zeta\rangle_z = \partial_x\langle\mathfrak{N}_y\rangle_z - \partial_y\langle\mathfrak{N}_x\rangle_z. \tag{9}$$

We can form wave equations similar to (8) for ρ and p_x. Letting $\mathcal{D}$ act on (7a) and (7b) yields

$$(\mathcal{D}^2 - c^2\nabla^2 + \kappa^2)\langle\rho\rangle_z + 2q\Omega\partial_y\langle p_x\rangle_z =$$
$$-2\Omega\langle\zeta\rangle_z - \partial_x\langle\mathfrak{N}_x\rangle_z - \partial_y\langle\mathfrak{N}_y\rangle_z \tag{10a}$$

and

$$(\mathcal{D}^2 - c^2\nabla^2 + \kappa^2)\langle p_x\rangle_z + 2q\Omega c^2\partial_y\langle\rho\rangle_z =$$
$$c^2\partial_y\langle\zeta\rangle_z + 2\Omega\langle\mathfrak{N}_y\rangle_z + \mathcal{D}\langle\mathfrak{N}_x\rangle_z. \tag{10b}$$

3.1 Decomposition into shearing waves

In the periodic shearing sheet we may expand all fluid variables in a series of plane wave solutions

$$\exp\left(\mathrm{i}k'_x x' + \mathrm{i}k'_y y'\right)$$

in the Lagrangian coordinate frame (6). Here, the radial and azimuthal wave numbers

$$k'_x = \frac{2\pi n_x}{L_x} \text{ and } k'_y = \frac{2\pi n_y}{L_y} \text{ with } n_x, n_y \in \mathbb{Z}.$$

In terms of Eulerian coordinates, the plane wave expansion for any (vertically averaged) fluid variable $\langle f \rangle_z$ reads

$$\langle f \rangle_z (x, y, t) = \sum_{n_x, n_y} \hat{f}(t) \exp\left[\mathrm{i}k_x(t)x + \mathrm{i}k_y y\right]$$

with a time dependent radial wave number

$$k_x(t) = k'_x + q\Omega t k'_y. \tag{11}$$

and constant azimuthal wave number $k_y = k'_y$.

When viewed from the Eulerian coordinate frame, the radial wave number of non-axisymmetric disturbances (for which $k_y \neq 0$) changes linearly in time due to advection by the linear shear, leading to the notion of sheared disturbances as originally discussed by Kelvin (Thomson 1887). In the shearing sheet, non-axisymmetric plane waves are therefore often referred to as shearing waves. In an astrophysical context, the usefulness of the concept of sheared disturbances for understanding accretion disk phenomena was first realised by Goldreich & Lynden-Bell (1965).

It is customary to classify shearing waves according to whether they are leading, i.e. $k_x(t)/k_y < 0$, or trailing, i.e. $k_x(t)/k_y > 0$. Because the time dependence of the radial wave number (11) is such that $k_x(t)/k_y$ always increases monotonically provided that $q\Omega > 0$, every leading wave will eventually become trailing as time progresses. The change from leading to trailing is referred to as 'swing' and occurs when $k_x(t) = 0$. Different shearing waves swing from leading to trailing at different times, successive swings being separated, for a given k_y, by a fixed time interval

$$\delta t_s = \frac{T_{\mathrm{orb}}}{q k_y L_x}, \tag{12}$$

where $T_{\mathrm{orb}} = 2\pi/\Omega$ is the orbital period.

We note that because we are dealing with the Fourier transforms of real quantities, each Fourier coefficient becomes equal to its complex conjugate under reflection of the wave number such that $\boldsymbol{k} \to -\boldsymbol{k}$. This means that we may without loss of generality consider only $k_y > 0$, and then multiply by a factor of two after taking the real part of the transforms to obtain physical quantities, which then accounts for $k_y < 0$. Thus from now on we consider only $k_y > 0$.

It is now straightforward to write down the SD wave equations (8) and (10) in Fourier space. Substituting

$$\mathcal{D} \to \mathrm{d}/\mathrm{d}t, \ \partial_x \to \mathrm{i}k_x(t), \text{ and } \partial_y \to \mathrm{i}k_y$$

we readily obtain

$$\frac{\mathrm{d}^2 \hat{\rho}}{\mathrm{d}t^2} + \left[\boldsymbol{k}^2(t)c^2 + \kappa^2\right]\hat{\rho} + 2q\Omega \mathrm{i}k_y \hat{p}_x =$$
$$- 2\Omega\hat{\zeta} - \mathrm{i}k_x(t)\hat{\mathfrak{N}}_x - \mathrm{i}k_y\hat{\mathfrak{N}}_y, \quad (13a)$$

$$\frac{\mathrm{d}^2 \hat{p}_x}{\mathrm{d}t^2} + \left[\boldsymbol{k}^2(t)c^2 + \kappa^2\right]\hat{p}_x + 2q\Omega c^2 \mathrm{i}k_y \hat{\rho} =$$
$$c^2 \mathrm{i}k_y \hat{\zeta} + 2\Omega\hat{\mathfrak{N}}_y + \frac{\mathrm{d}\hat{\mathfrak{N}}_x}{\mathrm{d}t}, \quad (13b)$$

and

$$\frac{\mathrm{d}^2 \hat{p}_y}{\mathrm{d}t^2} + \left[\boldsymbol{k}^2(t)c^2 + \kappa^2\right]\hat{p}_y = -c^2 \mathrm{i}k_x \hat{\zeta} + (q-2)\Omega\hat{\mathfrak{N}}_x + \frac{\mathrm{d}\hat{\mathfrak{N}}_y}{\mathrm{d}t}. \tag{13c}$$

3.2 Angular momentum flux

Conservation of angular momentum for linear waves in the shearing box follows from invariance of the system under translations along the azimuthal or y-direction. Here we note that this actually yields a momentum flux that can be converted into an angular momentum flux by multiplying by the radius of the centre of the box. As the latter quantity does not play any role in the box dynamics we can conveniently set it to be unity making the momentum and angular momentum fluxes equivalent. We introduce the Lagrangian displacement which we define through

$$\mathcal{D}\boldsymbol{\xi} = \boldsymbol{p}/\rho_0 - q\Omega\xi_x \boldsymbol{e}_y \tag{14}$$

In terms of $\boldsymbol{\xi}$, the density deviations from the background state are given by

$$\delta\rho/\rho_0 + \nabla \cdot \boldsymbol{\xi} = 0$$

and the linearised equations of motion become

$$\mathcal{D}^2\boldsymbol{\xi} = c^2\nabla\nabla \cdot \boldsymbol{\xi} - 2\boldsymbol{\Omega} \times \mathcal{D}\boldsymbol{\xi} + 2q\Omega^2\xi_x \boldsymbol{e}_x.$$

These also follow from the requirement that the action

$$S = \int \mathcal{L}(\boldsymbol{\xi}, \mathcal{D}\boldsymbol{\xi}, \nabla \cdot \boldsymbol{\xi})\,\mathrm{d}^3\boldsymbol{x}\,\mathrm{d}t,$$

$$S = \int \mathcal{L}\,\mathrm{d}^3\boldsymbol{x}\,\mathrm{d}t, \tag{15}$$

with the Lagrangian density given by

$$\mathcal{L} = \frac{\rho_0}{2}\left[\mathcal{D}\boldsymbol{\xi} \cdot \mathcal{D}\boldsymbol{\xi} - c^2(\nabla \cdot \boldsymbol{\xi})^2 + 2(\boldsymbol{\Omega} \times \boldsymbol{\xi}) \cdot \mathcal{D}\boldsymbol{\xi} + 2q\Omega^2\xi_x^2\right],$$

and the integral being taken over the box and between two arbitrary points in time, be stationary with respect to arbitrary variations of the Lagrangian displacement. The angular momentum conservation law follows from the invariance of the action (15) under infinitesimal translations in the y-direction. The resulting form of Noether's theorem yields

$$\mathcal{D}\left[\frac{\partial\mathcal{L}}{\partial(\mathcal{D}\boldsymbol{\xi})} \cdot \partial_y\boldsymbol{\xi}\right] + \nabla \cdot \left[\frac{\partial\mathcal{L}}{\partial(\nabla \cdot \boldsymbol{\xi})}\partial_y\boldsymbol{\xi} - \mathcal{L}\,\boldsymbol{e}_y\right] = 0.$$

We thus define the angular momentum density

$$A = -\frac{\partial\mathcal{L}}{\partial(\mathcal{D}\boldsymbol{\xi})} \cdot \partial_y\boldsymbol{\xi} = -\rho_0(\mathcal{D}\boldsymbol{\xi} + \boldsymbol{\Omega} \times \boldsymbol{\xi}) \cdot \partial_y\boldsymbol{\xi} \tag{16}$$

and the angular momentum flux

$$\boldsymbol{F} = -\frac{\partial\mathcal{L}}{\partial(\nabla \cdot \boldsymbol{\xi})}\partial_y\boldsymbol{\xi} + \mathcal{L}\,\boldsymbol{e}_y = -c^2\delta\rho\,\partial_y\boldsymbol{\xi} + \mathcal{L}\,\boldsymbol{e}_y, \tag{17}$$

which enables us to write

$$\mathcal{D}A + \nabla \cdot \boldsymbol{F} = 0. \tag{18}$$

Note the minus sign in equations (16) and (17) which can be determined from considering the action of an external force

(see also Ryu & Goodman 1992). The angular momentum conservation law (18) may be averaged over y and z to yield

$$\partial_t \langle A \rangle_{yz} + \partial_x \langle F_x \rangle_{yz} = 0.$$

The angular momentum flux as defined in (18) is, at times, inconvenient to work with because it involves the Lagrangian displacement $\boldsymbol{\xi}$. We can derive a related wave action where the radial flux only depends on mass density and momentum density as follows. From (7c) and (14) we have to linear order

$$\xi_x = \frac{p_y + c^2 \partial_y W}{(q-2)\Omega\rho_0}, \text{ where } \mathcal{D}W = \delta\rho. \qquad (19)$$

Inserting (19) into (17) yields after some straightforward algebra

$$F_x = \frac{c^2}{(2-q)\Omega\rho_0}$$
$$\left\{ \delta\rho\,\partial_y p_y + \partial_y\left(c^2\delta\rho\,\partial_y W\right) - \mathcal{D}\left[\frac{c^2}{2}\left(\partial_y W\right)^2\right] \right\}.$$

The second and the third term in curly brackets can be absorbed in the y-component of the angular momentum flux and in the angular momentum density, respectively, giving rise to a new wave action conservation law,

$$\mathcal{D}A' + \nabla \cdot \boldsymbol{F}' = 0,$$

where the modified radial angular momentum flux

$$F'_x = \frac{c^2\delta\rho\,\partial_y p_y}{(2-q)\Omega\rho_0}.$$

has the desired property that it does not involve the Lagrangian displacement. Furthermore, this new flux is equal to the radial component of the angular momentum flux (17) after averaging over y, z, and t. But it should be noted that it in order to establish this equality it has been assumed that no external forces act in the domain.

We will define a suitable temporal averaging procedure further below in Section 4.11. At this point we note that when evaluated for a single pair of (complex conjugate) shearing waves, and averaged over both y and z, the two equivalent expressions for the radial angular momentum flux become

$$\langle F_x \rangle_{yz} = -2k_y c^2 \text{Im}\left(\hat{\xi}_x^* \hat{\rho}\right) \qquad (20)$$

and

$$\langle F'_x \rangle_{yz} = \frac{2k_y c^2}{(2-q)\Omega\rho_0}\text{Im}\left(\hat{p}_y^* \hat{\rho}\right). \qquad (21)$$

Here, without loss of generality, we have adopted $k_y > 0$ as described in Section 3.1.

4 WKBJ THEORY OF WAVE EXCITATION

In this section we derive a WKBJ theory of the wave excitation that occurs during a swing cycle and derive an expression for the wave action produced. We go on to compare this theory in detail with the results of numerical integrations of the ordinary differential equations governing the time dependent evolution of the Fourier transforms of the wave amplitudes. Excellent agreement is obtained. In paper II we compare results obtained from the WKBJ theory with those obtained from MRI simulations.

4.1 The nature of the source terms

We first need to establish which of the source terms on the right hand sides of (13) are primarily responsible for wave excitation. Inspection of these equations shows that the source terms are of two kinds. The first kind is proportional to the transform of PPV and the second kind is proportional to the nonlinear stress tensor. Only terms of the first kind remain in the linear regime. Thus under conditions of weak nonlinearity, we would expect them to dominate. An analysis of the relative contributions found in direct simulations given in paper II shows that the contribution of the pseudo potential vorticity related terms is the more important by an order of magnitude confirming the above idea. It is also shown that the strength of the wave excitation phenomenon for a swinging wave is directly correlated with the amplitude of the pseudo potential vorticity transform at the time of the transition from leading to trailing. Here we reiterate that although the generation of PPV itself is driven by the nonlinear stresses, see (9), the linear source terms involving PPV survive at linear order if there is a build up over time under conditions of weak nonlinearity.

Following on from the above discussion, from now on we retain only source terms that depend on the pseudo potential vorticity. These are proportional to $\hat{\zeta}$ which we recall is a Fourier amplitude which is given by

$$\hat{\zeta}(t) = \frac{1}{L_x L_y} \int_0^{L_x}\int_0^{L_y} \langle \zeta \rangle_z (x,y,t) \, \exp\left[\mathrm{i}k_x(t)x + \mathrm{i}k_y y\right] \mathrm{d}x\,\mathrm{d}y$$

From the above expression we note that if $\langle \zeta \rangle_z (x,y,t)$ is an ultimately smooth function, the Riemann Lebesgue lemma allows us to infer that the source is negligible as $t \to \pm\infty$ and so is expected to peak when the wave swings from leading to trailing. Thus the wave amplitude excitation process should also be localized around this time.

At this point we recall that in a shearing box the wave excitation process for a fixed k_y appears as a succession of swings, which as seen from (11) are separated by the time interval (12). For the longest possible wave length in the y direction given by the box size this is $L_y/(2\pi q L_x)$ orbital periods. This is independent of the box size as long as the aspect ratio is fixed. Although this time interval formally decreases as L_x increases, because of the periodic symmetry associated with the shearing box, we expect results to be independent of L_x once this is larger than the radial correlation length associated with the turbulence, expected to be $\sim H$. Accordingly we might expect the phenomenon to take a similar form in global simulations (e.g. Nelson 2005).

4.2 Reduction to three uncoupled second order oscillator equations

As motivated above we will now neglect any nonlinearities in the problem. After dropping the nonlinear source terms appearing in the SD wave equations (8) and (10) the evolution of ρ, p_x, and p_y in Fourier space is governed by

$$\frac{\mathrm{d}^2\hat{\rho}}{\mathrm{d}t^2} + \left(\boldsymbol{k}^2 c^2 + \kappa^2\right)\hat{\rho} + 2q\Omega\mathrm{i}k_y\hat{p}_x = -2\Omega\hat{\zeta}, \qquad (22a)$$

$$\frac{\mathrm{d}^2\hat{p}_x}{\mathrm{d}t^2} + \left(\boldsymbol{k}^2 c^2 + \kappa^2\right)\hat{p}_x + 2q\Omega c^2\mathrm{i}k_y\hat{\rho} = c^2\mathrm{i}k_y\hat{\zeta}, \qquad (22b)$$

and

$$\frac{\mathrm{d}^2\hat{p}_y}{\mathrm{d}t^2} + \left(\boldsymbol{k}^2c^2 + \kappa^2\right)\hat{p}_y = -c^2\mathrm{i}k_x\hat{\zeta}. \tag{23}$$

We note that in the absence of nonlinearities the pseudo potential vorticity,

$$\hat{\zeta} = \mathrm{i}k_x\hat{p}_y - \mathrm{i}k_y\hat{p}_x + (q-2)\Omega\hat{\rho}, \tag{24}$$

is conserved exactly, i.e.

$$\frac{\mathrm{d}\hat{\zeta}}{\mathrm{d}t} = 0. \tag{25}$$

The wave equation for $\hat{p}_y$, given by (23), therefore decouples from those for $\hat{\rho}$ and $\hat{p}_x$, given by (22). The latter two equations may be decoupled from each other as well by introducing the pair

$$\hat{p}_\pm = \hat{p}_x \pm \hat{\rho}c, \tag{26}$$

for which the linearised wave equations read

$$\frac{\mathrm{d}^2\hat{p}_\pm}{\mathrm{d}t^2} + \left(\boldsymbol{k}^2c^2 + \kappa^2 \pm 2q\Omega\mathrm{i}k_yc\right)\hat{p}_\pm = c\left(\mathrm{i}k_yc \mp 2\Omega\right)\hat{\zeta}. \tag{27}$$

We reiterate that the above equations describe the excitation of density waves and accordingly it may be confirmed that they are absent in the incompressible limit for which $c \to \infty$ while maintaining time derivatives finite. In this limit, it is readily verified from (22) and (23) that the excited or forced flow considered below simply becomes the incompressible flow associated with a vorticity distribution that is slowly varying through the action of nonlinear MHD forces. We note the pseudo potential vorticity becomes the vorticity in that limit.

We can simplify (23) and (27) further by introducing the dimensionless time variable

$$\tau = \frac{k_xc}{\sqrt{k_y^2c^2 + \kappa^2}} \tag{28}$$

and the dimensionless parameter

$$\epsilon = \frac{q\Omega k_yc}{k_y^2c^2 + \kappa^2} \tag{29}$$

in terms of which we have

$$\epsilon^2\frac{\mathrm{d}^2\hat{p}_y}{\mathrm{d}\tau^2} + (\tau^2 + 1)\hat{p}_y = -c\left(\frac{\mathrm{i}k_xc}{k_y^2c^2 + \kappa^2}\right)\hat{\zeta} \tag{30a}$$

and

$$\epsilon^2\frac{\mathrm{d}^2\hat{p}_\pm}{\mathrm{d}\tau^2} + (\tau^2 + 1 \pm 2\mathrm{i}\epsilon)\hat{p}_\pm = c\left(\frac{\mathrm{i}k_yc \mp 2\Omega}{k_y^2c^2 + \kappa^2}\right)\hat{\zeta}. \tag{30b}$$

We remark that the homogeneous form of these equations with $\hat{\zeta} = 0$ can be solved in terms of Parabolic Cylinder functions (e.g. Narayan et al. 1987). However, we did not find this feature to be useful in the context of this paper. Rather we use the fact that the form of the inhomogeneous equations suggests an asymptotic expansion in ϵ. Formally, such an expansion is valid if $\epsilon \ll 1$. From (29) we can see that this will be the case both in the high and the low azimuthal wave number limit given by $k_yc \gg \kappa$ and $k_yc \ll \kappa$, respectively.

In the following, we will derive asymptotic solutions to (30) based on the smallness of ϵ. However, we will demonstrate that these approximative solutions show excellent agreement with the exact solution obtained from direct numerical integration even in the worst possible case of $k_yc = \kappa$ for which ϵ attains its maximum value, $\epsilon^{\max} = q\Omega/2\kappa$.

4.3 Slowly varying solutions

We consider equations (30) for large $|\tau|$, i.e. in the high radial wave number limit. In this limit the second time derivatives are significant only for solutions that vary rapidly in τ. Such solutions are expected when sources are absent and correspond to high frequency oscillations. This suggests that they can be dropped for solutions that vary slowly with τ. As a first approximation, we drop the double time derivative in (30) to obtain

$$\bar{p}_y = -c\left(\frac{\mathrm{i}k_xc}{\boldsymbol{k}^2c^2 + \kappa^2}\right)\hat{\zeta} \tag{31a}$$

and

$$\bar{p}_\pm = c\left(\frac{\mathrm{i}k_yc \mp 2\Omega}{\boldsymbol{k}^2c^2 + \kappa^2 \pm 2q\Omega\mathrm{i}k_yc}\right)\hat{\zeta}, \tag{31b}$$

where we have used (28) and (29). These approximative solutions to inhomogeneous problem are the leading order terms of an asymptotic series expansion in ascending powers of ϵ. The series diverges near the time of the swing from leading to trailing, i.e. near $\tau = 0$, when the double time derivative in (30) becomes significant and oscillatory solutions to the homogeneous equation must be taken into account.

The occurrence of such oscillatory solutions may easily be demonstrated by direct numerical integration of (30), which is just a set of linear ordinary differential equations. We start the integration in the far leading phase, i.e. at $\tau = \tau_0$ with τ_0 large and negative. In this limit the balanced solutions (31) hold and may be used as initial conditions. We note that in doing so we have to be careful not to violate PPV conservation which we know to be exact in linear theory, see (25). This problem arises on account of the additional time derivative taken to obtain (8) and (10) from (7).

Formally, the balanced solutions (31) are reconcilable with PPV conservation only in the limit $\tau \to \pm\infty$. We thus introduce an error if we use these solutions as initial conditions at some finite τ_0 and we have to make sure that τ_0 is sufficiently large so that this error is small. In order to be able to quantify this error during the course of the integration, we express the PPV $\hat{\zeta}$ in terms of $\hat{\rho}$ and $\hat{p}_x$, see (24) together with (26), and solve (30) as a system of three coupled ordinary differential equations. (Alternatively, equations (7) could be solved directly). PPV conservation is not guaranteed in this case, but we find empirically that the numerical integration conserves PPV arbitrarily well depending on how large τ_0 (and thus the error introduced by using the balanced solutions as initial conditions) is.

Bearing these general remarks in mind, we now discuss a specific numerical solution to (30). For this purpose we consider Keplerian shear, i.e. $q = 3/2$. Because we would like to determine empirically how well asymptotic theory works when we are far away from the asymptotic limit $\epsilon \ll 1$ we take the worst possible case, i.e. a shearing wave with $k_y = \kappa/c = 1/H$ so that $\epsilon = q\Omega/2\kappa = 3/4$. For the determination of the initial conditions from the balanced solutions we assume, without loss of generality, that $\hat{\zeta} = \Omega\rho_0$ in (31).

We start the integration at $\tau = -100$.[2] The evolution

---

[2] At this point the relative error as far as PPV conservation is concerned is $\sim 10^{-8}$. We find that the relative error never exceeds
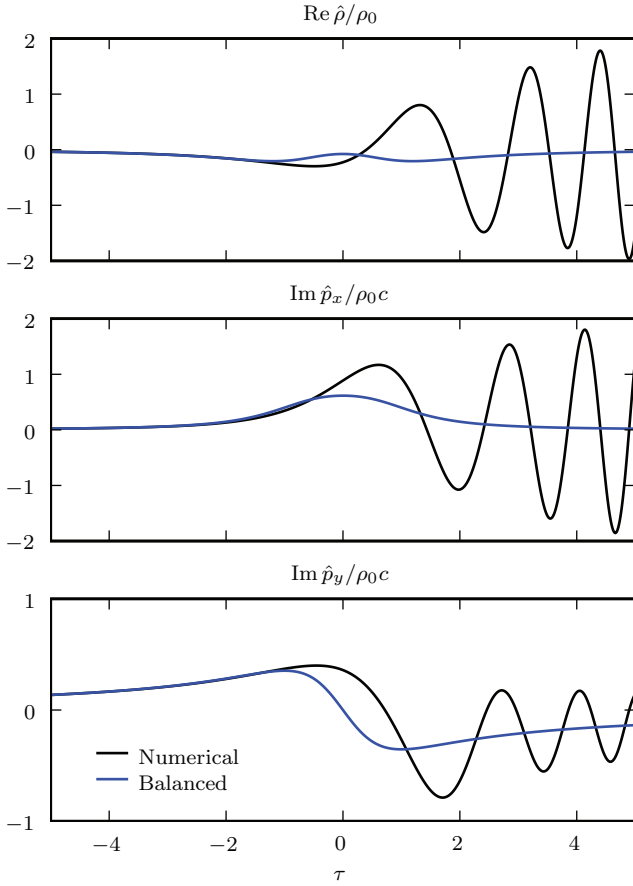
Figure 1. Comparison between the numerical solution (black) to the linearised wave equations (30) with the corresponding balanced solutions (blue). Here we have used (26) to compute $\hat{\rho}$ and $\hat{p}_x$ from $\hat{p}_\pm$. The parameters in this example are $q = 3/2$, $\epsilon = 3/4$, and $\hat{\zeta} = \Omega \rho_0$.

of the Fourier amplitudes near the swing from leading to trailing as a function of the radial wave number is shown in Fig. 1. Before the swing from leading to trailing the numerical solution closely follows the balanced solution up until $\tau \approx 0$ where a sudden transition to oscillatory behaviour occurs. In the trailing phase, the numerical solution oscillates with a relatively large but rather slowly evolving amplitude around the balanced solution. Such oscillatory behaviour cannot be captured by a perturbation series expansion. In order to describe it we have to resort to singular perturbation theory to be discussed in the next section.

4.4 WKBJ solution of the generic oscillator equation

To study the excitation of a general Fourier mode we seek a solution to the forced harmonic oscillator equation of the general type

$$\epsilon^2 \frac{d^2 y(\tau)}{d\tau^2} + (\tau^2 + a^2)y(\tau) = f(\tau) \tag{32}$$

10^{-6} during the entire course of the integration from $\tau = -100$ to $\tau = 10$.

with $\epsilon \ll 1$ and where a is a complex number with

$$|a| \sim O(1) \quad \text{and} \quad |\text{ph}\, a| < \pi/4, \tag{33}$$

the latter being true for $a = \sqrt{1 + 2i\epsilon}$ with $0 \leqslant \epsilon < \infty$.

Throughout the following analysis make $w = z^{1/n}$ single-valued by taking the branch cut along the negative real axis and always take the principal branch, thus

$$\text{ph}\, w = \frac{\text{ph}\, z}{n}. \tag{34}$$

We note that equations (30a) and (30b) are special cases of the above general form. We further also assume that $f(\tau)$ is a slowly varying function such that $\Delta f \sim O(1)$ for $\Delta \tau \sim O(1)$ as $\epsilon \to 0$. Physically this means that the pseudo potential vorticity transform should vary at a slow rate compared to the wave oscillation frequency at around the time of the swing. This is expected under conditions of weak nonlinearity as discussed in section 4.1 and simulation results presented in paper II indicate that this is indeed the case.

4.5 Outer and balanced solutions

A solution of equation (32) in ascending powers of ϵ^2 is readily found from regular perturbation theory, and yields to lowest order

$$y(\tau) = \frac{f(\tau)}{\tau^2 + a^2} + O(\epsilon^2), \tag{35}$$

which is, given (33), well defined on the entire real axis. However, this series, giving rise to what is described as the balanced solution, is only asymptotic. At all orders in ϵ^2, the series will fail to represent rapidly changing oscillatory contributions to $y(\tau)$ for which the double derivative term in (32) is significant. These vanish more rapidly than any power of ϵ as $\epsilon \to 0$.

In order to obtain these contributions, that are in fact associated with the excited SD waves, we have to resort to singular perturbation theory. We thus seek a solution of the asymptotic form

$$y(\tau) \approx \frac{f(\tau)}{\tau^2 + a^2}, \qquad\qquad \tau \to -\infty \tag{36}$$

$$y(\tau) \approx \frac{f(\tau)}{\tau^2 + a^2} + \frac{A_+ e^{-i\Phi(\tau)/\epsilon}}{(\tau^2 + a^2)^{1/4}} + \frac{A_- e^{+i\Phi(\tau)/\epsilon}}{(\tau^2 + a^2)^{1/4}}, \quad \tau \to +\infty \tag{37}$$

which is the sum of the leading order solution to the inhomogeneous problem obtained from regular perturbation theory, and a standard WKBJ solution to the homogeneous problem. Here the WKBJ phase is given by

$$\Phi(\tau) = \int_0^\tau \sqrt{\sigma^2 + a^2}\, d\sigma$$
$$= \frac{1}{2}\left[\tau \sqrt{\tau^2 + a^2} + a^2 \ln\left(\frac{\tau + \sqrt{\tau^2 + a^2}}{\sqrt{a^2}} \right) \right]. \tag{38}$$

4.6 Matching on anti-Stokes lines

In order to determine the WKBJ (or wave) amplitudes A_+ and A_-, we analytically continue the WKBJ solution (37) into the complex τ-plane and match it to inner solutions

valid in the immediate vicinity of the two complex WKBJ turning points at $\tau_* = \pm ia$. Thus in this section the $\pm$ alternative refers to the turning point with positive and negative imaginary part respectively rather than the $\hat{p}_\pm$ alternative of the previous section.

We find it convenient to match inner and outer solutions along the so-called anti-Stokes lines defined by

$$\operatorname{Im}\Phi(\tau) = \operatorname{Im}\Phi(\tau_*). \qquad (39)$$

Because the imaginary part of the WKBJ phase is constant on these lines, one of the WKBJ exponentials in (37) is maximally sub-dominant to the other one and may thus be ignored.

From the first order Taylor expansion about a turning point we have

$$\tau^2 + a^2 \approx 2\tau_*(\tau - \tau_*) \qquad (40)$$

and therefore from equation (38) we obtain

$$\Phi(\tau) \approx \Phi(\tau_*) + \frac{2\sqrt{2}}{3}\tau_*^{1/2}(\tau - \tau_*)^{3/2}$$

The condition (39) thus defines three anti-Stokes lines emanating from each turning point at angles given by

$$\operatorname{ph}(\tau - \tau_*) = \left(\mp\frac{5\pi}{6}, \mp\frac{\pi}{6}, \pm\frac{\pi}{2}\right) - \frac{\operatorname{ph}a}{3}$$

For consistency we match on the anti-Stokes lines originating from each turning point that asymptotically approach the real axis.

For $\operatorname{Re}\tau < \operatorname{Re}(\pm ia)$ these are

$$\operatorname{ph}(\tau - \tau_*) = \mp\frac{5\pi}{6} - \frac{\operatorname{ph}a}{3} \qquad (41)$$

and for $\operatorname{Re}\tau > \operatorname{Re}(\pm ia)$

$$\operatorname{ph}(\tau - \tau_*) = \mp\frac{\pi}{6} - \frac{\operatorname{ph}a}{3} \qquad (42)$$

Note that with the definition of the square root obtained from (34), the WKBJ solution (37) has branch cuts that leave the turning points at an angle

$$\operatorname{ph}(\tau - \tau_*) = \pm\frac{\pi}{2} - \operatorname{ph}a$$

so we can always match along the anti-Stokes lines specified above without crossing branch cuts. This is illustrated in Fig. 2.

On an anti-Stokes line one of the two WKBJ exponentials in (37) will be maximally sub-dominant to the other in the limit $\epsilon \to 0$, depending on the sign of the imaginary part of the WKBJ phase at the turning point from which it emanates. At these we have

$$\Phi(\pm ia) = \pm ia^2\pi/4$$

and thus when the conditions (33) are satisfied

$$\operatorname{Im}\Phi(\pm ia) \gtrless 0.$$

This means in general that the maximally sub-dominant exponential has an amplitude smaller by a factor $\propto \exp(-c_0/\epsilon)$, where c_0 is a constant of order unity when compared to the dominant one, which is very small for small ϵ. Therefore it should be neglected. Dropping the maximally sub-dominant WKBJ exponential, in the vicinity of
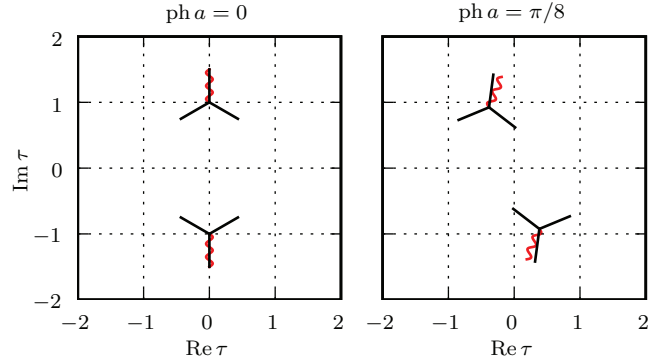

Figure 2. Anti-Stokes lines (solid black) emanating from the two turning points for $\operatorname{ph}a = 0$ (left panel) and $\operatorname{ph}a = \pi/8$ (right panel). The curly red curves indicate branch cuts.
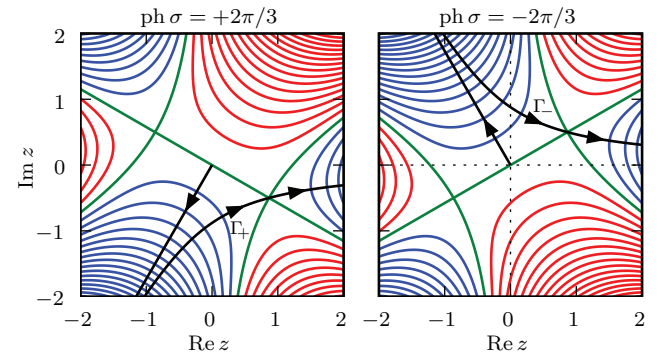

Figure 3. Integration contours for the Airy-integral (47) in the z plane. In each case the contour is deformed from the positive real axis to the two paths shown. These contours (black), which extend to infinity, correspond to the situation where we are on the anti-Stokes lines that radiate away from the turning points towards the positive real axis on which $\operatorname{ph}\sigma = 2\pi/3$ at the upper turning point (left panel) and $\operatorname{ph}\sigma = -2\pi/3$ at the lower turning point (right panel).

the turning points our WKBJ solution is to leading order in $\tau \mp ia$

$$y(\tau) \sim \frac{f(\tau_*)}{2\tau_*(\tau - \tau_*)} + \frac{A_\pm e^{\pi a^2/4\epsilon}}{[2\tau_*(\tau - \tau_*)]^{1/4}}$$
$$\exp\left[\mp i\epsilon^{-1}\frac{2\sqrt{2}}{3}\tau_*^{1/2}(\tau - \tau_*)^{3/2}\right]$$

We see that matching on the anti-Stokes line emanating from the upper (lower) turning point will only enable us to determine the WKBJ amplitude A_+ (A_-). We will thus need to match on the anti-Stokes lines from both turning points in order to determine the full WKBJ solution.

4.7   Inner solution

To obtain the inner solutions we consider the governing equation (32) in the vicinity of the turning points. Using the first order Taylor expansion around a turning point (40) this becomes

$$\epsilon^2\frac{d^2y(\tau)}{d\tau^2} + 2\tau_*(\tau - \tau_*)y(\tau) = f(\tau_*). \qquad (43)$$

We now defined rescaled variables through

$$\sigma = e^{\pm 2\pi i/3}(2\tau_*)^{1/3}\epsilon^{-2/3}(\tau - \tau_*) \qquad (44)$$

$$y(\tau) = e^{\pm 2\pi i/3}(2\tau_*)^{-2/3}\epsilon^{-2/3}f(\tau_*)\phi(\sigma) \qquad (45)$$

The first of these indicates that the solutions we seek vary on a scale $|\tau| \sim \epsilon^{2/3} \ll 1$. This feature enables us to perform an asymptotic expansion valid for large $|\sigma|$ and still remain in the vicinity of the turning points. In terms of the rescaled variables, equation (43) yields an inhomogeneous Airy-type equation

$$\frac{d^2\phi(\sigma)}{d\sigma^2} + \sigma\phi(\sigma) = 1. \qquad (46)$$

We remark that from equation (44) we deduce that

$$\text{ph}\,\sigma = 0 \quad \text{for} \quad \text{ph}(\tau - \tau_*) = \mp\frac{5\pi}{6} - \frac{\text{ph}\,a}{3}$$

which applies on the anti-Stokes lines given by (41) and

$$\text{ph}\,\sigma = \pm\frac{2\pi}{3} \quad \text{for} \quad \text{ph}(\tau - \tau_*) = \mp\frac{\pi}{6} - \frac{\text{ph}\,a}{3}$$

which applies on the anti-Stokes lines given by (42).

4.8 Integral representation for the inner solutions

The solution to (46) can be written as an integral

$$\phi(\sigma) = \int_0^\infty e^{h(\sigma,z)}dz \quad \text{with} \quad h(\sigma,z) = -\sigma z - z^3/3. \quad (47)$$

We are interested in the large-σ asymptotic behaviour of this solution, which is applicable on each of the anti-Stokes lines emanating from both turning points.

For the anti-Stokes lines corresponding to $\text{ph}\,\sigma = 0$ we integrate along the positive real axis and get an end-point contribution via Watson's lemma

$$\phi(\sigma) \sim \frac{1}{\sigma} \quad (\sigma \to \infty, \ \text{ph}\,\sigma = 0)$$

or with (44) and (45)

$$y(\tau) \sim \frac{f(\tau_*)}{2\tau_*(\tau - \tau_*)}$$

which matches our outer solution (37) to the left of the turning points if there we set $A_+ = A_- = 0$ consistent with the causality requirement of the lack of existence of excited waves for $\tau \to -\infty$.

For the anti-Stokes lines corresponding to $\text{ph}\,\sigma = \pm 2\pi/3$ we deform the integration contour from the positive real axis to a contour consisting of two separate line segments, writing

$$\int_0^\infty e^{h(\sigma,z)}dz = \int_0^{\infty\,e^{\mp 2i\pi/3}} e^{h(\sigma,z)}dz + \int_{\Gamma_\pm} e^{h(\sigma,z)}dz. \quad (48)$$

The first integral on the right hand side is evaluated along a straight line that goes from the origin to $\infty e^{\mp 2\pi i/3}$. Along this line, $h(z)$ is purely real and negative, and we again get an end-point contribution via Watson's lemma,

$$\int_0^{\infty\,e^{\mp 2i\pi/3}} e^{h(z)}dz \sim \frac{1}{\sigma}$$

$$(\sigma \to \infty, \ \text{ph}\,\sigma = \pm 2\pi/3).$$

The curve $\Gamma_\pm$ along which the second integral on the right

hand side of (48) is taken goes from $\infty\,e^{\mp 2\pi i/3}$ along a path of steepest descent through the saddle point $z_s = \mp i\sigma^{1/2}$ and from there to ∞, see Fig. 3. In the limit $\sigma \to \infty$, most of the contribution to this integral will come from near the saddle point z_s, at which $h(z_s) = \pm(2/3)i\sigma^{3/2}$ and so

$$\int_{\Gamma_\pm} e^{h(z)}dz \sim \frac{\pi^{1/2}e^{\pm(2/3)i\sigma^{3/2}}}{e^{\mp\pi i/4}\sigma^{1/4}}$$

$$(\sigma \to \infty, \ \text{ph}\,\sigma = \pm 2\pi/3).$$

We thus have

$$\phi(\sigma) \sim \frac{1}{\sigma} + \frac{\pi^{1/2}e^{\pm(2/3)i\sigma^{3/2}}}{e^{\mp i\pi/4}\sigma^{1/4}}$$

$$(\sigma \to \infty, \ \text{ph}\,\sigma = \pm 2\pi/3).$$

Using (44) and (45) we may reexpress the above solution in terms of y and $\tau - \tau^*$ to obtain

$$y(\tau) \sim \frac{f(\tau_*)}{2\tau_*(\tau - \tau_*)} + \frac{e^{\pm 3\pi i/4}(\pi/\epsilon)^{1/2}f(\tau_*)}{(2\tau_*)^{3/4}(\tau - \tau_*)^{1/4}}$$

$$\exp\left[\mp i\epsilon^{-1}\frac{2\sqrt{2}}{3}\tau_*^{1/2}(\tau - \tau_*)^{3/2}\right]$$

We match this solution to our outer solution (37) in the neighbourhood of each turning point by equating the factors in front of the maximally dominant WKBJ exponentials. This then yields the amplitudes

$$A_\pm = \pm i f(\pm ia)\left(\frac{\pi}{2a\epsilon}\right)^{1/2}e^{-\pi a^2/4\epsilon}.$$

Using these, the full asymptotic solution takes the form

$$y(\tau) \approx \frac{f(\tau)}{\tau^2 + a^2} + \left(\frac{2\pi}{a\epsilon}\right)^{1/2}\frac{e^{-\pi a^2/4\epsilon}}{(\tau^2 + a^2)^{1/4}}$$

$$\frac{1}{2i}\left[f(-ia)\,e^{+i\Phi(\tau)/\epsilon} - f(+ia)\,e^{-i\Phi(\tau)/\epsilon}\right]. \quad (49)$$

4.9 Determination of the wavelike forms of $\hat{p}_y$, $\hat{p}_\pm$, $\tilde{p}_x$, and $\tilde{\rho}$

We are now in a position to obtain explicit solutions for $\hat{p}_y$ and $\hat{p}_\pm$. To bring the wave equation (30a) for $\hat{p}_y$ into the form of the general oscillator equation (32) we set

$$a = 1 \quad \text{and} \quad f(\tau) = -\frac{ic\tau\hat{\zeta}}{\sqrt{k_y^2 c^2 + \kappa^2}}.$$

To obtain the wavelike part of the solution, i.e. the component proportional to the WKBJ exponential, which we will denote by a tilde, $f(\tau)$ has to be evaluated at the complex turning point τ_*. Because PPV is conserved in linear theory this poses no difficulties and we immediately obtain

$$\tilde{p}_y = \frac{i\hat{\zeta}_s c}{\sqrt{k_y^2 c^2 + \kappa^2}}\sqrt{\frac{2\pi}{\epsilon}}\frac{e^{-\pi/4\epsilon}}{(\tau^2 + 1)^{1/4}}\cos\left[\Phi(\tau)/\epsilon\right], \quad (50)$$

where $\hat{\zeta}_s = \hat{\zeta}(0)$ denotes the PPV amplitude and the time of the swing and the WKBJ phase

$$\Phi(\tau) = \frac{1}{2}\left[\tau\sqrt{\tau^2 + 1} + \ln\left(\tau + \sqrt{\tau^2 + 1}\right)\right]. \quad (51)$$

Using the definitions of τ and ϵ, respectively given by (28) and (29), we can rewrite the solution for $\tilde{p}_y$ as

$$\tilde{p}_y = iH\hat{\zeta}_s\mathcal{A}\sqrt{\Omega/\omega}\cos\left(\int_0^t \omega\,dt'\right), \quad (52)$$

where the dimensionless amplitude

$$\mathcal{A} = \frac{\Omega^{1/2}}{(k_y^2 c^2 + \kappa^2)^{1/4}} \sqrt{\frac{2\pi}{\epsilon}} \, \mathrm{e}^{-\pi/4\epsilon} \qquad (53)$$

and we have defined the SD wave frequency

$$\omega = \sqrt{\boldsymbol{k}^2 c^2 + \kappa^2}.$$

This procedure is readily repeated to obtain explicit solutions for $\hat{p}_\pm$. In this case, comparison of the governing equation (30b) with (32) implies that we need to set

$$a = \sqrt{1 \pm 2\mathrm{i}\epsilon} \quad \text{and} \quad f(\tau) = c\left(\frac{\mathrm{i}k_y c \mp 2\Omega}{k_y^2 c^2 + \kappa^2}\right)\hat{\zeta}$$

The solutions for $\tilde{p}_\pm$ determined from (49) are thus

$$\tilde{p}_\pm = \mathrm{i}\hat{\zeta}_{\mathrm{s}} c \left(\frac{2\Omega \mp \mathrm{i}k_y c}{k_y^2 c^2 + \kappa^2}\right) \frac{1}{(1 \pm 2\mathrm{i}\epsilon)^{1/4}}$$
$$\sqrt{\frac{2\pi}{\epsilon}} \frac{\mathrm{e}^{-\pi/4\epsilon}}{(\tau^2 + 1 \pm 2\mathrm{i}\epsilon)^{1/4}} \sin\left(\Phi_\pm/\epsilon\right), \quad (54)$$

where the WKBJ phase

$$\Phi_\pm = \frac{1}{2}\left[\tau\sqrt{\tau^2 + 1 \pm 2\mathrm{i}\epsilon} + \right.$$
$$\left. (1 \pm 2\mathrm{i}\epsilon)\ln\left(\frac{\tau + \sqrt{\tau^2 + 1 \pm 2\mathrm{i}\epsilon}}{\sqrt{1 \pm 2\mathrm{i}\epsilon}}\right)\right].$$

It is important to note here that $\Phi_\pm$ are not real with the consequence that quantities such as $\mathrm{e}^{\mathrm{i}\Phi_+/\epsilon}$ have a power law as well as exponential dependence on τ for large τ.

Again, we rewrite (54) in more familiar terms using (28) and (29) to obtain

$$\tilde{p}_\pm = \mathrm{i}\hat{\zeta}_{\mathrm{s}} H \mathcal{A}_\pm \sqrt{\Omega/\omega_\pm} \sin\left(\int_0^t \omega_\pm \, \mathrm{d}t'\right), \qquad (55)$$

where this time the amplitude is given by

$$\mathcal{A}_\pm = \frac{\Omega^{1/2}}{(k_y^2 c^2 + \kappa^2 \pm 2q\Omega\mathrm{i}k_y c)^{1/4}}$$
$$\left(\frac{2\Omega \mp \mathrm{i}k_y c}{\sqrt{k_y^2 c^2 + \kappa^2}}\right)\sqrt{\frac{2\pi}{\epsilon}} \, \mathrm{e}^{-\pi/4\epsilon} \quad (56)$$

and the wave frequency is

$$\omega_\pm = \sqrt{\omega^2 \pm 2q\Omega\mathrm{i}k_y c}.$$

Note that both the amplitude and the wave frequency are complex valued.

Recalling that $\hat{p}_\pm = \hat{p}_x \pm \hat{\rho}c$, it is now a simple matter to determine the wavelike contributions to $\hat{p}_x$ and $\hat{\rho}$ in the forms

$$\tilde{\rho} = -\hat{\zeta}_{\mathrm{s}}\Omega^{-1} \mathrm{Im}\left[\mathcal{A}_+\sqrt{\Omega/\omega_+} \sin\left(\int_0^t \omega_+ \, \mathrm{d}t'\right)\right] \qquad (57a)$$

and

$$\tilde{p}_x = \mathrm{i}\hat{\zeta}_{\mathrm{s}} H \, \mathrm{Re}\left[\mathcal{A}_+\sqrt{\Omega/\omega_+} \sin\left(\int_0^t \omega_+ \, \mathrm{d}t'\right)\right] \qquad (57b)$$

where we have used the fact that $\mathcal{A}_+ = \mathcal{A}_-^*$ and $\omega_+ = \omega_-^*$.

We have seen in Section 4.3 that the balanced solutions (31) show good agreement with the exact numerical solution in the leading phase but fail to capture the oscillatory behaviour in the trailing phase. Having derived the wave like WKBJ solutions of the homogeneous wave equations, i.e.
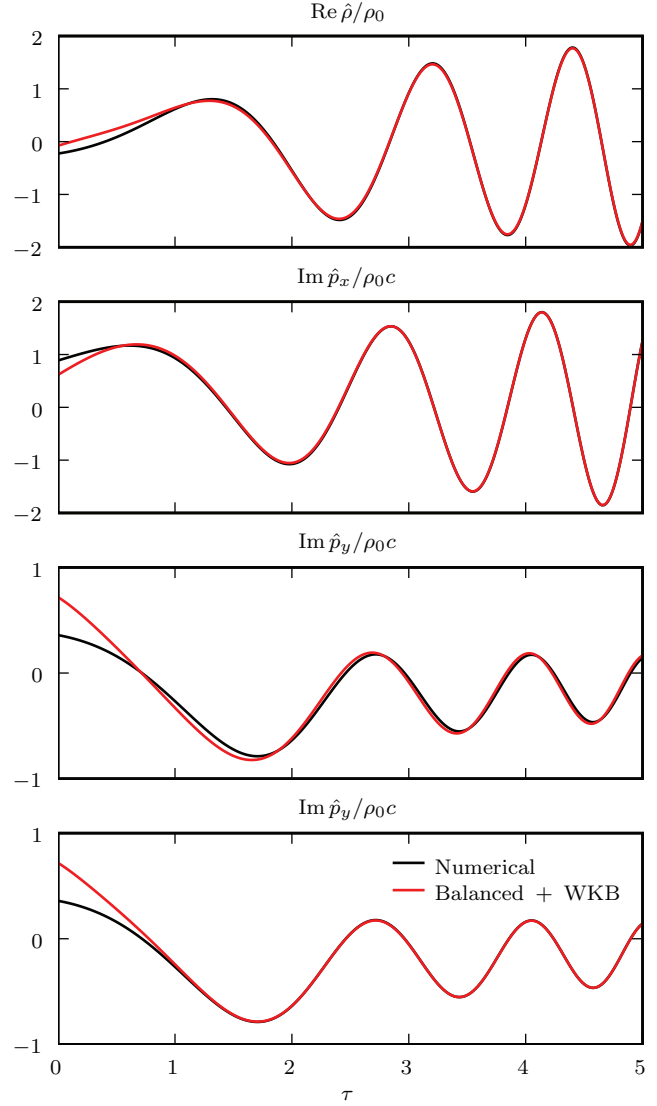

Figure 4. Comparison between the numerical solution (black) to the linearised wave equations (30) with the full asymptotic, i.e. balanced plus WKBJ, solution (red). The parameters are the same as in Fig. 1, i.e. $q = 3/2$, $\epsilon = 3/4$, and $\hat{\zeta} = \Omega\rho_0$. In the lowermost panel, $\hat{p}_y$ was obtained from (58), while in the panel immediately above it was obtained from (52).

(52), (57a) and (57b), we are now in a position to determine whether they correctly describe this oscillatory behaviour.

In Fig. 4 we compare the exact numerical solution discussed in Section 4.3 with the full asymptotic solution, i.e. the sum of the balanced and the WKBJ solution, in the trailing phase ($\tau > 0$). There is excellent agreement between the full asymptotic solutions and the numerical solutions. Beyond $\tau = 2$ the asymptotic solutions are virtually indistinguishable from the numerical solutions. Remarkably, this is so even though for this example we have chosen a shearing wave with an intermediate azimuthal wave number of $k_y c = \kappa$ for which the 'small' parameter ϵ attains its maximum value, $\epsilon = 3/4$ in the case of Keplerian shear considered here, and we are therefore as far away as possible from the asymptotic limit $\epsilon \ll 1$.

We note that in the case of $\hat{p}_y$ there is a small but noticable discrepancy between the numerical solution and the full asymptotic solution obtained directly from (52). However, we can derive an alternative expression for $\hat{p}_y$ from PPV conservation. Because the WKBJ solutions are solutions to the free wave equations they should carry no PPV, from which it follows that

$$\tilde{p}_y = \frac{\mathrm{i}k_y\tilde{p}_x + (2-q)\Omega\tilde{\rho}}{\mathrm{i}k_x} \tag{58}$$

This expression agrees with (52) in the limit $\epsilon \ll 1$ and we see from Fig. 4 that (58) is in fact more accurate for $\epsilon \sim 1$.

We comment that after we have reintroduced the spatial dependence by multiplying with $\exp(\mathrm{i}\boldsymbol{k}\cdot\boldsymbol{x})$ and then taking the real part, these solutions are found to consist of two waves of equal amplitude travelling in opposite directions. This is a natural outcome given the symmetries of the shearing box. However, for the same reason, both waves transport angular momentum in the same direction, i.e. outward if they are trailing, see Section 4.11.

4.10 Asymptotic behaviour of the WKBJ solutions

The WKBJ solutions for $\tilde{\rho}$ and $\tilde{p}_x$ given by (57a) and (57b), respectively, involve complex phases which disguises their large time asymptotic behaviour. To make this more apparent we note that for large times or equivalently τ we have

$$\Phi_+ \sim \Phi + \mathrm{i}\epsilon\left[\frac{1}{2} + \ln(2\tau)\right] - \frac{(1+2\mathrm{i}\epsilon)\ln(1+2\mathrm{i}\epsilon)}{4},$$

where Φ is given by equation (51) and is purely real. We see that the imaginary part of Φ_+ will result in an extra power of τ when taking the exponential. This has the consequence that when the sine of the WKBJ phase in (57a) and (57b) is re-expressed in terms of exponentials only those with absolute values that increase with τ need to be retained. In this case these are $\propto \exp(-\mathrm{i}\Phi_+/\epsilon)$ and their asymptotic form is given by

$$\exp\left(-\mathrm{i}\Phi_+/\epsilon\right) \sim 2\tau \exp\left(-\mathrm{i}\Phi/\epsilon\right)$$
$$\frac{1}{\sqrt{1+2\mathrm{i}\epsilon}}\exp\left[\frac{1}{2} - \frac{\ln(1+2\mathrm{i}\epsilon)}{4\mathrm{i}\epsilon}\right],$$

from which it follows that

$$\sin\left(\int_0^t \omega_+\,\mathrm{d}t'\right) \sim \mathrm{i}\left(\frac{\omega}{\Omega}\right)\exp\left(-\mathrm{i}\int_0^t\omega\,\mathrm{d}t'\right)\frac{\mathcal{B}_+}{\mathcal{A}_+},$$

where we have defined

$$\mathcal{B}_+ = \frac{\Omega\,\mathcal{A}_+}{\sqrt{k_y^2c^2 + \kappa^2 + 2q\Omega\mathrm{i}k_yc}}\exp\left[\frac{1}{2} - \frac{\ln(1+2\mathrm{i}\epsilon)}{4\mathrm{i}\epsilon}\right]. \tag{59}$$

Using the above relations we can readily find the large τ asymptotic forms of $\tilde{\rho}$ and $\tilde{p}_x$ given by

$$\tilde{\rho} \sim -\hat{\zeta}_{\mathrm{s}}\Omega^{-1}|\mathcal{B}_+|\sqrt{\omega/\Omega}\cos\left(\int_0^t\omega\,\mathrm{d}t' - \mathrm{ph}\,\mathcal{B}_+\right) \tag{60a}$$

and

$$\tilde{p}_x \sim \mathrm{i}\hat{\zeta}_{\mathrm{s}}H|\mathcal{B}_+|\sqrt{\omega/\Omega}\sin\left(\int_0^t\omega\,\mathrm{d}t' - \mathrm{ph}\,\mathcal{B}_+\right). \tag{60b}$$

We thus see that because the WKBJ amplitudes for $\tilde{\rho}$ and $\tilde{p}_x$ are complex valued, see (56), the envelope of the oscillation grows in time and there is non-trivial phase shift with respect to $\tilde{p}_y$.

4.11 The angular momentum flux

In section 3.2 we obtained two equivalent expressions for the radial angular momentum flux F_x which uses the radial Lagrangian displacement and F_x' which uses the y-component of the momentum density. We determined the angular momentum flux for a single pair of (complex conjugate) shearing waves. Here, we are interested in the angular momentum flux associated with the excited waves, i.e. with the WKBJ solutions. In (20) and (21) we therefore replace $\hat{\rho}$, $\hat{p}_y$, $\hat{\xi}_x$ by $\tilde{\rho}$, $\tilde{p}_y$, $\tilde{\xi}_x$, respectively, and obtain

$$\langle F_x\rangle_{yz} = -2k_yc^2\mathrm{Im}\left(\tilde{\xi}_x^*\tilde{\rho}\right) \tag{61}$$

and

$$\langle F_x'\rangle_{yz} = \frac{2k_yc^2}{(2-q)\Omega\rho_0}\mathrm{Im}\left(\tilde{p}_y^*\tilde{\rho}\right), \tag{62}$$

where $k_y > 0$ is understood.

We can use the WKBJ solutions just obtained to determine these angular momentum fluxes. In order to calculate (61) we need an explicit expression for the radial Lagrangian displacement which in Fourier space is given by

$$\hat{\xi}_x = \frac{1}{\rho_0}\int\hat{p}_x\,\mathrm{d}t.$$

the leading order WKBJ solution in the limit of large τ can be calculated from (60b) directly and is given by

$$\tilde{\xi}_x \sim -\frac{\mathrm{i}\hat{\zeta}_{\mathrm{s}}H}{\Omega\rho_0}\sqrt{\Omega/\omega}\,|\mathcal{B}_+|\cos\left(\int_0^t\omega\,\mathrm{d}t' - \mathrm{ph}\,\mathcal{B}_+\right)$$

Using this result together with (60a) we readily obtain

$$\lim_{\tau\to\infty}\overline{\langle F_x\rangle}_{yz} = \frac{k_yc|\hat{\zeta}_{\mathrm{s}}|^2H^2|\mathcal{B}_+|^2}{\Omega\rho_0}.$$

With the help of (56) and (59) this may be expressed in the form

$$\lim_{\tau\to\infty}\overline{\langle F_x\rangle}_{yz} = \frac{2\pi|\hat{\zeta}_{\mathrm{s}}|^2H^2}{q\rho_0}\frac{\Omega(k_y^2c^2 + 4\Omega^2)\,\mathrm{e}^{f(\epsilon)}\,\mathrm{e}^{-\pi/2\epsilon}}{\left[(k_y^2c^2 + \kappa^2)^2 + (2q\Omega k_yc)^2\right]^{3/4}}, \tag{63}$$

where the overline denotes an average over one oscillation period, and we have defined

$$f(\epsilon) = 1 - \frac{\tan^{-1}(2\epsilon)}{2\epsilon}.$$

Alternatively, we may use equation (62) to determine the wave action. This involves $\tilde{p}_y$ instead of $\tilde{\xi}_x$ and is accordingly easier to work with in an Eulerian formulation. The calculation of (62) is cumbersome if we use the 'direct' WKBJ solution for $\hat{p}_y$, given by (52), because its non-trivially phase shifted with respect to the WKBJ solutions for $\hat{\rho}$ and $\hat{p}_x$, given by (57a) and (57b), making the temporal average over one oscillation period somewhat ill defined. However, if we exploit PPV conservation and express $\hat{p}_y$ in terms of $\hat{\rho}$ and $\hat{p}_x$, see (58), which is also found to be more accurate for $\epsilon \sim 1$ (see Fig. 4), the calculation is trivial and we obtain

$$\lim_{\tau\to\infty}\overline{\langle F_x'\rangle}_{yz} = \lim_{\tau\to\infty}\overline{\langle F_x\rangle}_{yz}. \tag{64}$$

In Fig. 5 we show the angular momentum flux $\langle F_x'\rangle$ associated with the wave parts of solutions plotted in Fig. 4. In order to obtain the wave part of the numerical solution we have simply subtracted the balanced solution.
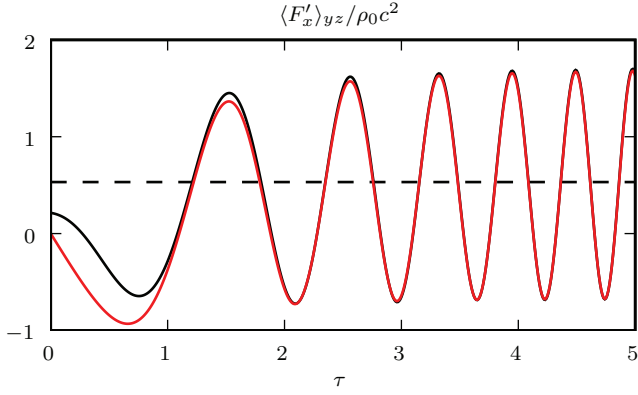
Figure 5. Wave action for the wave shown in Fig. 4. The black and red line are the wave action for the wave part of the numerical and WKBJ solution, respectively. The dashed line indicates the large-τ average value (63).

Figure 6. Exponential dependence of the WKBJ amplitudes on the azimuthal wave number k_y for a Keplerian rotation law.

As expected, the WKBJ solutions agrees with the numerical solution remarkably well. Due to interference between the forward and the backwards travelling waves actually obtained in our numerical solution, the quantity defined by (62) oscillates. However, the average over one oscillation period approaches a constant non-zero value as is expected for a linear wave.

5   DISCUSSION

In this paper we have developed a theory of SD wave excitation in a rotating shear flow with turbulence which may result from the magneto-rotational instability but under the assumption that the magnetic field is too weak to affect the form of the waves significantly. We considered the commonly adopted shearing box model for which the flow is subject to the boundary condition of periodicity in shearing coordinates (Goldreich & Lynden-Bell 1965).

The main feature resulting from the shear is that wave excitation occurs through a sequence of regularly spaced swings as the wave changes from leading to trailing form. For a fixed azimuthal wave number k_y, and a Keplerian rotation profile, the swings are separated by a time interval $\delta t_s = T_{orb}/(qk_yL_x)$, where the orbital period $T_{orb} = 2\pi/\Omega$. For the optimal azimuthal wave number $k_y = \kappa/c$ (see discussion below) and $L_x = H$ as an estimated radial correlation length of the turbulence, which should also be the minimum box size required to capture its essential properties, it follows that $\delta t_s \approx T_{orb}$.

The wave equations governing the excitation during a particular swing were found to depend on time alone and under the assumption that the important source terms causing the wave excitation are associated with the pseudo potential vorticity, they could be solved to find the asymptotic wave form and net positive wave action produced. The form of the wave equations necessitated a WKBJ analysis in the complex plane. In this respect the formalism differs from shearing box analyses that adopt rigid or free boundary conditions, or which assume strictly harmonic forcing with radial boundaries extended to infinity, rather than periodicity in shearing coordinates. In the former cases one can sepa-
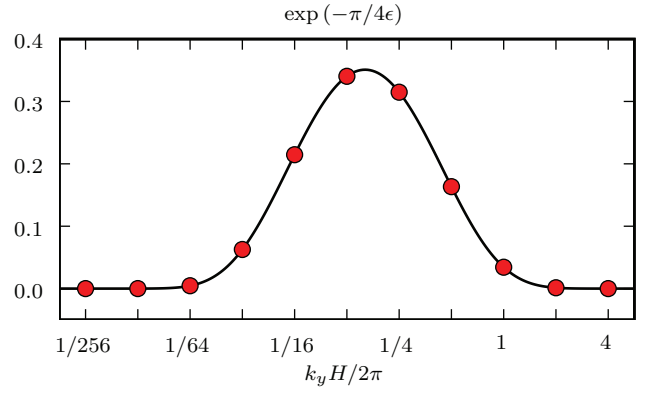
rate out a harmonic time dependence and solve a problem in space for the wave amplitude (e.g. Narayan et al. 1987).

The analysis of the wave excitation process driven by pseudo potential vorticity carried out in this paper has similarities to an analysis of inertia-gravity waves excited in the earth's atmosphere by Vanneste & Yavneh (2004) who perform an analogous WKBJ analysis in the complex plane.

The excitation process produces waves of equal amplitude propagating in opposite directions. As these waves are both trailing, by symmetry each produces an equal outward angular momentum flow. Even when the excitation process is linear, as the waves propagate away, the radial wave length shortens until shock dissipation eventually occurs (e.g. Goodman & Rafikov 2001). Thus waves are always likely to be seen to manifest nonlinear effects as the characteristic radial wave length shortens. When waves behave linearly during the initial excitation, but subsequently undergo significant but not complete dissipation between successive swings, the rate of angular momentum transport can be estimated as the wave action produced in single swing given by equation (63). This situation is found to occur in the simulations presented in paper II.

An important parameter is the value of the azimuthal/horizontal wave number, k_y, for which the wave excitation is most favoured, which we define as being the value for which the wave amplitude produced is maximal. According to (52) and (55) the wave amplitude is a product of a known function of k_y and the square of the Fourier amplitude of PPV at the time of swing. The latter quantity, being determined by the nonlinear hydromagnetic turbulence, cannot be found from the wave excitation calculations performed here. This aspect is discussed in paper II where relevant numerical simulations are performed and analysed. Here we shall anticipate results and assume that the PPV spectrum is relatively flat at small k_y with the consequence that it does not affect the dependence of the wave amplitude on k_y significantly.

The wave amplitude depends on the azimuthal wave number k_y through the parameter

$$\epsilon = \frac{q\Omega k_y c}{k_y^2 c^2 + \kappa^2}$$

in such a way that it is exponentially small for $\epsilon \ll 1$, see (53) and (56). Given the fact that ϵ is small both in the

small and the long azimuthal wave number limit, we deduce that wave excitation will be most effective near the optimal wave number

$$k_y^{\mathrm{opt}} = \kappa/c$$

for which ϵ takes its maximum value

$$\epsilon_{\max} = q\Omega/(2\kappa).$$

For a Keplerian disc with $q = 3/2$ and $\kappa = 1$ we have $k_y^{\mathrm{opt}} = 1/H$ and thus $\epsilon_{\max} = 3/4$. We recall that WKBJ theory gives very accurate results for values of ϵ as large as this. For illustrative purposes we plot the exponential dependence of the wave amplitudes as a function of azimuthal wave number in Fig. 6. We see that amplitude of the excited wave falls off rapidly away from the optimal wave number.

The arguments given above suggest that SD wave production will be most effective for $k_y \sim k_y^{\mathrm{opt}}$. This is the longest possible azimuthal wave length for a box with $L_y = 2\pi H$ as is commonly adopted. For boxes of this size and smaller wave production is expected to be most effective at the longest azimuthal wave length. On the other hand once L_y exceeds $2\pi H$ the longest wave length is expected to no longer be the most effective. This is fully supported by the simulation results presented in paper II. In this paper we confirm the main features of the excitation process described here and verify the dominance of the pseudo potential vorticity related source terms. Although the waves are observed to become nonlinear very soon after the initial excitation, the main features of the analysis presented here are confirmed. This suggests that useful extensions can be made to the analysis of wave excitation under more general conditions such as those that incorporate significant self-gravity. We plan to undertake these in the near future.

REFERENCES

Armitage P. J., 1998, ApJ, 501, L189+
Balbus S. A., Hawley J. F., 1991, ApJ, 376, 214
Balbus S. A., Hawley J. F., 1998, Reviews of Modern Physics, 70, 1
Bodo G., Chagelishvili G., Murante G., Tevzadze A., Rossi P., Ferrari A., 2005, A&A, 437, 9
Chagelishvili G. D., Tevzadze A. G., Bodo G., Moiseev S. S., 1997, Physical Review Letters, 79, 3178
Fromang S., Papaloizou J., 2007, A&A, 468, 1
Gardiner T. A., Stone J. M., 2005, in de Gouveia dal Pino E. M., Lugones G., Lazarian A., eds, Magnetic Fields in the Universe: From Laboratory and Stars to Primordial Structures. Vol. 784 of American Institute of Physics Conference Series, Energetics in MRI driven Turbulence. pp 475–488
Goldreich P., Lynden-Bell D., 1965, MNRAS, 130, 125
Goodman J., Rafikov R. R., 2001, ApJ, 552, 793
Heinemann T., Papaloizou J. C. B., 2009, MNRAS, in press
Johnson B. M., Gammie C. F., 2005, ApJ, 626, 978
Lighthill M. J., 1952, Royal Society of London Proceedings Series A, 211, 564
Lin D. N. C., Papaloizou J. C. B., 1996, ARA&A, 34, 703
Narayan R., Goldreich P., Goodman J., 1987, MNRAS, 228, 1
Nelson R. P., 2005, A&A, 443, 1067
Nelson R. P., Papaloizou J. C. B., 2004, MNRAS, 350, 849
Oishi J. S., Mac Low M.-M., Menou K., 2007, ApJ, 670, 805
Papaloizou J. C. B., Lin D. N. C., 1995, ARA&A, 33, 505
Ryu D., Goodman J., 1992, ApJ, 388, 438
Shakura N. I., Syunyaev R. A., 1973, A&A, 24, 337
Shen Y., Stone J. M., Gardiner T. A., 2006, ApJ, 653, 513
Thomson W., 1887, Philos. Mag, 24, 188
Vanneste J., Yavneh I., 2004, Journal of Atmospheric Sciences, 61, 211